Effects of single- and multi-substituted Zn ions in doped 122-type iron-based superconductors

YuanYuan Zhao,[1] Bo Li,[1] Wei Li,[2] Hong-Yi Chen,[1,3] Kevin E. Bassler,[1] and C. S. Ting[1]

[1]*Department of Physics and Texas Center for Superconductivity, University of Houston, Houston, Texas 77204, USA*

[2]*State Key Laboratory of Functional Materials for Informatics and Shanghai Center for Superconductivity, Shanghai Institute of Microsystem and Information Technology, and CAS-Shanghai Science Research Center, Chinese Academy of Sciences, Shanghai 200050, China*

[3]*National Taiwan Normal University, Department of Physics, Taipei 116, Taiwan*

Recent experiments on Zn-substituted 122-type iron-based superconductors (FeSCs) at electron- and hole-doped regions provide us with a testing ground for understanding the effect of Zn impurities in these systems. Our first-principles calculations of the electronic structure reveal that the Zn $3d$ orbitals are far below the Fermi level and are chemically inactive, while the Zn $4s$ orbital is partially occupied and its wave function overlaps with the $3d$ orbitals of neighboring Fe ions. This suggests that the impurity effect originates in the Zn $4s$ orbital, not its $3d$ orbitals. Employing a phenomenological two-orbital lattice model for 122-FeSCs and the self-consistent Bogoliubov–de Gennes equations, we study how the Zn impurities suppress the superconductivity in electron- and hole-doped compounds. Our obtained results qualitatively agree with the experimental measurements.

I. INTRODUCTION

In iron-based superconductors (FeSCs), doping can be made by partial substitution of Co and Ni for Fe [1,2], or substitution of K and Na for Ba [3,4] in antiferromagnetic (AFM) parent compounds. With increased doping, the spin-density-wave (SDW) order is suppressed and superconductivity (SC) emerges. In addition, the nonmagnetic impurity could be regarded as an important probe in understanding pairing symmetry in superconductors. According to Anderson's theorem [5,6], nonmagnetic impurities may not cause pair breaking in conventional s-wave superconductors, but they severely suppress the SC transition temperature T_c in d-wave [7] and $s_\pm$-wave [8,9] superconductors. Studying the effect due to nonmagnetic impurities in FeSCs becomes an indispensable avenue to understand the superconducting physics in these compounds.

In 122-FeSCs, Zn substitution for the Fe ion is preferred as an ideal nonmagnetic impurity [10–13]. Most recently, Li *et al.* reported [14] that SC can barely survive with 3% Zn substitutions in hole-doped $Ba_{0.5}K_{0.5}Fe_2As_2$. They also showed that the local destruction of SC may provide evidence for s-wave pairing symmetry, while the measurements [15,16] in electron-doped $BaFe_{1.89-2x}Zn_{2x}Co_{0.11}As_2$ demonstrate that the SC is completely suppressed above a concentration of roughly 8% Zn, regardless of whether the sample is in the underdoped, optimally doped, or overdoped regimes. On the other hand, the experimentally observed T_c suppression is much slower than that predicted by the theory for the $s_\pm$-wave pairing state [9]. A recent work [12] by Chen *et al.* appears to be able to account for the suppression of SC at roughly 8% Zn in optimally electron-doped 122-FeSCs. So far, a theory which is able to consistently explain the different T_c suppressions for electron- and hole-doped 122-FeSCs is missing. In order to understand this difference, we reexamine the nature of Zn impurities by first-principles calculations and construct a model to describe the substituted Zn in $BaFe_2As_2$.

The Zn element has a $3d^{10}4s^2$ electronic configuration. Generally, it is divalent in compounds. Similar to earlier studies [17–20], our first-principles calculations [21], as shown in Fig. 1(a), demonstrate that Zn $3d$ states are far below the Fermi energy, by about 8 eV. In addition, our calculations demonstrate that the peaks of the Zn $4s$ level are narrowly distributed above and below the Fermi energy. More importantly, the empty Zn $4s$ level is not far above the Fermi energy, which suggests that Zn $4s$ orbitals are partially occupied and Zn does not have a valence of 2. Thus the heterovalent doping effect of substituted Zn should be considered in the system.

The conventional way of treating substituted Zn [12,13] in the mean-field frame is to assume that overlapping exists between Zn $3d$ and its neighboring Fe $3d$ orbitals. Meanwhile, in order to reflect that the Zn $3d$ level is far below the Fermi energy, a strongly negative potential-scattering term is assigned at the Zn site. According to our first-principles calculations, the fully occupied $3d$ orbitals of the substituted-Zn impurity should be regarded to be strongly localized, and that they do not contribute to the electron density of states near the Fermi energy. The partially occupied $4s$ orbital of substituted Zn should be the only orbital responsible for impurity scattering. Instead of considering Zn $3d$ orbitals, we study the effect due to its $4s$ orbital. Because the energy of the empty Zn $4s$ level is close to the Fermi energy, it should be reasonable to choose a scattering potential of intermediate strength at the Zn site.

In this paper, we use an effective two-orbital tight-binding model [25,26] to describe the $BaFe_2As_2$ system without substituted Zn. For substituted Zn, there is only one $4s$ orbital, so we have to adjust the hopping parameters between Zn and the adjacent Fe sites. These parameters are chosen to fit the experimental results for optimally electron-doped 122-FeSCs [15,16]. Then we employ the fixed parameters to study the T_c suppressions for electron-doped 122-FeSCs at the underdoped region and for the hole-doped 122-FeSCs. Employing self-consistent lattice Bogoliubov–de Gennes (BdG) equations, we demonstrate that our obtained results are qualitatively comparable with those experiments [14–16] on T_c suppressions in various 122-FeSCs with substituted Zn.
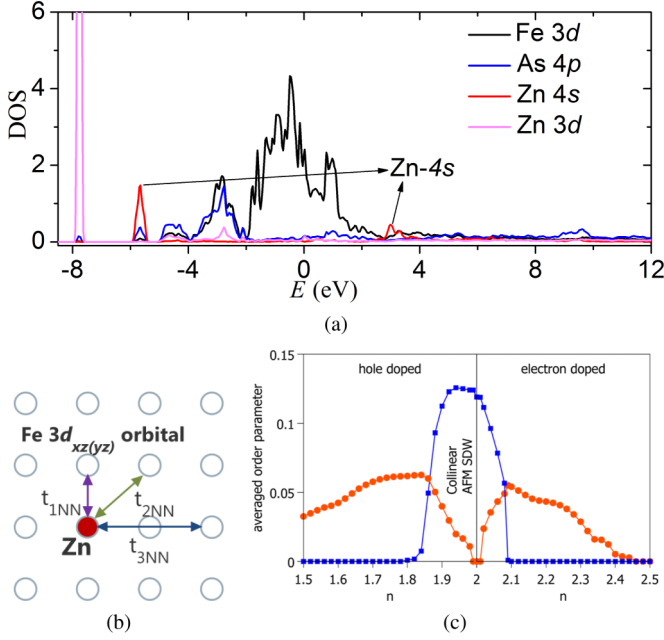
FIG. 1. (a) Partial Fe $3d$, Zn $3d$, Zn $4s$, and As $4p$ density of states in substituted $BaFe_2As_2$ [21]. (b) The schematic diagram of the Zn-Fe hopping integrals between the Zn $4s$ orbital and Fe $3d_{xz(yz)}$ orbital. The red solid circle represents the substituted-Zn ion and the gray circles represent the Fe ions. The purple, green, and blue solid lines correspond to the first-nearest-neighbor (1NN), second-nearest-neighbor (2NN), and third-nearest-neighbor (3NN) hopping terms, respectively. (c) Averaged magnetic and SC order parameters change under different doping levels n for the $BaFe_2As_2$ compound.

II. MODEL CONSTRUCTION

In the following, we discuss the details of our model for performing the calculations. In the parent compound $BaFe_2As_2$, the Fe ions form a square lattice, while the As anions sit alternatively below and above the center of each plaquette of the Fe lattice. This structure contains two intertwined sublattices of Fe ions, denoted by A and B. Heretofore there are several microscopic multiorbital models that describe iron-based superconductors [25–33]. We choose an effective model [26], which has been tested by capturing several important features of the $BaFe_2As_2$ compounds, in good agreement with experiments. This two-orbital tight-binding model takes into account of two Fe ions per unit cell, and each of the Fe includes $3d_{xz}$ and $3d_{yz}$ orbitals. It has also been proven that this model can represent within one Fe atom per unit cell after a gauge transformation [12]. The full Hamiltonian of the $BaFe_2As_2$ system can be written as

$$H = H_{BCS} + H_{int} + H_{imp}. \tag{1}$$

Here, H_{BCS} is the BCS-type Hamiltonian, including the hopping term and the pairing term, expressed as

$$H_{BCS} = \sum_{i,j,\alpha,\beta,\sigma} t_{ij}^{\alpha\beta} c_{i\alpha\sigma}^\dagger c_{j\beta\sigma} - \sum_{i,\alpha,\sigma} \mu c_{i\alpha\sigma}^\dagger c_{i\alpha\sigma}$$
$$+ \sum_{i,j,\alpha} V_{ij}(\langle c_{i\alpha\downarrow} c_{j\alpha\uparrow}\rangle c_{i\alpha\downarrow}^\dagger c_{j\alpha\uparrow}^\dagger + \text{H.c.}), \tag{2}$$

where $c_{i\alpha\sigma}^\dagger$ and $c_{i\alpha\sigma}$ are, respectively, the creation and annihilation operators for an electron with spin σ in the orbitals $\alpha = 1$ or 2 on the ith lattice site, and μ is the chemical potential which is determined by the electron filling per site, corresponding to different doping. $t_{ij}^{\alpha\beta}$ are the hopping integrals. We choose the nonvanishing hopping elements as [12,26] $t_{\pm\hat{x}}^{\alpha\bar\alpha} = t_{\pm\hat{y}}^{\alpha\bar\alpha} = t_1$, $t_{\pm(\hat{x}+\hat{y})}^{11} = t_{\pm(\hat{x}-\hat{y})}^{22} = t_2$, $t_{\pm(\hat{x}-\hat{y})}^{11} = t_{\pm(\hat{x}+\hat{y})}^{22} = t_3$, $t_{\pm(\hat{x}\pm\hat{y})}^{\alpha\alpha} = t_4$, $t_{\pm\hat{x}}^{\alpha\alpha} = t_{\pm\hat{y}}^{\alpha\alpha} = t_5$, and $t_{\pm 2\hat{x}}^{\alpha\alpha} = t_{\pm 2\hat{y}}^{\alpha\alpha} = t_6$.

Also, $V_{ij}\langle c_{i\alpha\downarrow} c_{j\alpha\uparrow}\rangle = \Delta_{ij}^{\alpha}$ is the SC bond pairing order parameter between site i and j. Here, we only consider the next-nearest-neighbor (NNN) intraorbital pairing with strength $V_{ij} = V_{NNN} = V$, as a constant. This choice is consistent with the $s_\pm$ pairing [34–36] and has been widely used in previous theoretical studies based on the BdG technique [37,38].

H_{int} is the on-site interaction term. At the mean-field level, it can be written as

$$H_{int} = U \sum_{i,\alpha,\sigma\neq\bar\sigma} \langle \hat{n}_{i\alpha\bar\sigma}\rangle \hat{n}_{i\alpha\sigma} + U' \sum_{i,\alpha\neq\beta,\sigma\neq\bar\sigma} \langle \hat{n}_{i\alpha\bar\sigma}\rangle \hat{n}_{i\beta\sigma}$$
$$+ (U' - J_H) \sum_{i,\alpha\neq\beta,\sigma} \langle \hat{n}_{i\alpha\sigma}\rangle \hat{n}_{i\beta\sigma}, \tag{3}$$

where $\hat{n}_{i\alpha\sigma} = c_{i\alpha\sigma}^\dagger c_{i\alpha\sigma}$. The orbital rotation symmetry imposes the constraint $U' = U - 2J_H$ [39].

The impurity part of the Hamiltonian H_{imp} includes two parts, expressed as

$$H_{imp} = \sum_{I_m\sigma} V_{imp} c_{I_m\sigma}^\dagger c_{I_m\sigma} + \sum_{I_m j\alpha\sigma} (\tilde{t}_{I_m j}^{s\alpha} c_{I_m\sigma}^\dagger c_{j\alpha\sigma} + \text{H.c.}), \tag{4}$$

where $c_{I_m\sigma}^\dagger$ and $c_{I_m\sigma}$ are, respectively, the creation and annihilation operators for an electron with spin σ on the (I_m)th lattice site. The original Fe ion at the (I_m)th lattice site is substituted by a Zn ion. The first part of Eq. (4) represents the on-site scattering. V_{imp} is the scattering strength. Here, $V_{imp} > 0$, which suggests that the Zn impurities behave as randomly distributed local-potential barriers embedded in a sea of itinerant electrons.

Based on the spherical spatial orientation of the Zn orbital, the hopping integrals $\tilde{t}_{I_m j}^{s\alpha}$ between the α orbital of the adjacent Fe ion at the jth lattice site and the s orbital of the substituted-Zn ion at the (I_m)th lattice site should be isotropic along different directions. As shown in Fig. 1(b), we suppose the hopping terms between the substituted-Zn ion and adjacent Fe ions include first-nearest-neighbor (1NN) t_{1NN}, second-nearest-neighbor (2NN) t_{2NN}, and third-nearest-neighbor (3NN) t_{3NN}. For convenience, without introducing new parameters into our model, their strengths are chosen to be $t_{1NN} = t_5$, $t_{2NN} = t_3$, and $t_{3NN} = t_6$.

Now, we write down the matrix form of Eq. (1) with the basis $\psi_{i\alpha} = (c_{i\alpha\uparrow}, c_{i\alpha\downarrow}^\dagger)^T$, $H = \sum_{ij\alpha\beta} \psi_{i\alpha}^\dagger H_{BdG} \psi_{j\beta}$, and calculate the eigenvalues and eigenvectors of H_{BdG}:

$$\sum_{j\beta} \begin{pmatrix} H_{ij\uparrow}^{\alpha\beta} & \Delta_{ij}^{\beta} \\ \Delta_{ij}^{\beta*} & -H_{ij\downarrow}^{\alpha\beta} \end{pmatrix} \begin{pmatrix} u_{j\beta}^n \\ v_{j\beta}^n \end{pmatrix} = E_n \begin{pmatrix} u_{i\alpha}^n \\ v_{i\alpha}^n \end{pmatrix}, \tag{5}$$

where $H_{ij\sigma}^{\alpha\beta} \equiv [H_{\text{BCS}} + H_{\text{int}} + H_{\text{imp}}]_{ij\sigma}^{\alpha\beta}$, is the matrix element for the single-particle Hamiltonian, and we have

$$\Delta_{ij}^{\alpha} = \frac{V_{ij}}{4} \sum_n \left(u_{i\alpha}^n v_{j\alpha}^{n*} + u_{j\alpha}^n v_{i\alpha}^{n*} \right) \tanh\left(\frac{E_n}{2k_B T} \right), \quad (6)$$

$$\langle \hat{n}_{i\alpha\uparrow} \rangle = \sum_n |u_{i\alpha}^n|^2 f(E_n),$$

$$\langle \hat{n}_{i\alpha\downarrow} \rangle = \sum_n |v_{i\alpha}^n|^2 [1 - f(E_n)], \quad (7)$$

$$\langle \hat{n}_{i\alpha} \rangle = \langle \hat{n}_{i\alpha\uparrow} \rangle + \langle \hat{n}_{i\alpha\downarrow} \rangle.$$

Here, $f(E_n)$ is the Fermi-Dirac distribution function. To facilitate the discussion of physical quantities, we define the local magnetization and the $s_{\pm}$-wave projection of the SC order parameter at each site i, respectively, as $m_i = \frac{1}{4} \sum_\alpha (\langle \hat{n}_{i\alpha\uparrow} \rangle - \langle \hat{n}_{i\alpha\downarrow} \rangle)$, $\Delta_i = \frac{1}{8} \sum_{\delta,\alpha} \Delta_{ii+\delta}^\alpha$, where $\delta \in \{\pm\hat{x} \pm \hat{y}\}$. In addition, we also calculate the averaged values of $\langle |M| \rangle = \frac{1}{N} \sum_i |m_i|$ and $\langle \Delta_s \rangle = \frac{1}{N} \sum_i \Delta_i$, where N is the number of Fe sites in the real-space lattice.

As mentioned before, substituted Zn plays a heterovalent doping role in the system. The electron filling $n \equiv n_{\text{Zn-free}}$ represents the original level of a Zn-free system, which varies with the increase of substituted Zn. For each constituent of $\text{Ba}(\text{Fe}_{1-x}\text{Zn}_x)_2\text{As}_2$, once the original doping level is determined, the total electrons in the system are initialized to the summation of the electrons (n) at the Fe sites, and the electrons are provided at the substituted Zn ($4s^2$). In our self-consistent calculations of each specific doping level (n) and Zn concentration ratio (x), we set the total electron number of our system to be unchangeable, and the chemical potential is determined by the total electron filling.

Throughout the paper, the energy is measured in units of t_5. The temperature is set to be $T = 0.0001$. The six hopping integrals are $t_{1-6} = (0.09, 0.08, 1.35, -0.12, -1.00, 0.25)$. The on-site Coulomb interaction U and Hund's coupling J_H are set to be 3.5 and 0.4, respectively. The pairing strength $V = 1.3$. With these parameters, the dependence of the averaged magnetic and SC order parameters on the doping is illustrated in Fig. 1(c), which is consistent with the experimental results [40,41]. We choose the scattering strength of impurity $V_{\text{imp}} = 3$. The numerical calculations are performed on a 28×28 square lattice with periodic boundary conditions. In the multi-impurity cases, at each doping level n and Zn-concentration value x, we calculate at least 20 different impurity configurations, in each of which the substituted ions are distributed randomly. Furthermore, we try to avoid an excessive concentration of impurities in a certain area. All the results we present have been checked by using different initial values. Those results remain qualitatively similar, indicating the reliability of our calculations.

III. LOCAL ELECTRON DENSITY AND LOCAL DENSITY OF STATES (LDOS) AROUND SUBSTITUTED ZINC

With $V_{\text{imp}} = 3$–4, the local electron density at the substituted-Zn ion is around 1. For convenience, we choose $V_{\text{imp}} = 3$ in our calculations. Figure 2 shows the spatial profile of the local electron density under different conditions. At a
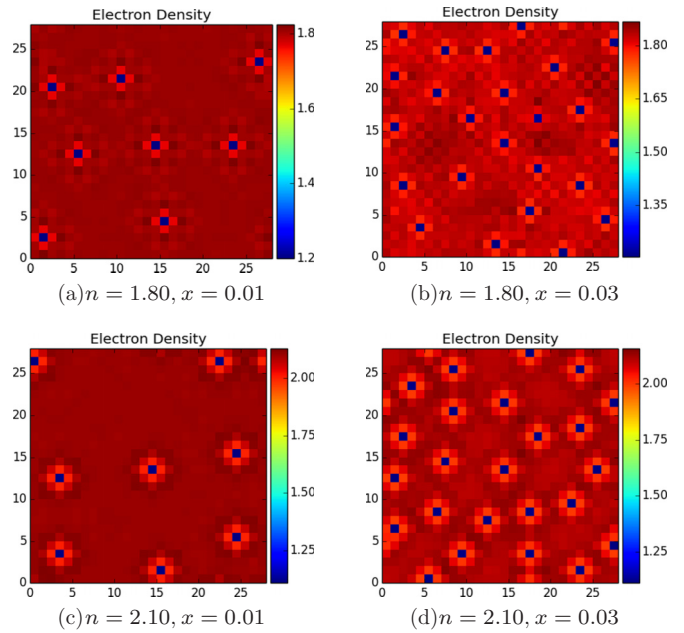
FIG. 2. Spatial profiles of local electron density at different doping levels (n) and different Zn-concentration ratios x. (a) $n = 1.80$, $x = 0.01$; (b) $n = 1.80$, $x = 0.03$; (c) $n = 2.10$, $x = 0.01$; (d) $n = 2.10$, $x = 0.03$.

specific doping level n, the local electron density around the substituted-Zn impurities changes just a little with different x.

In order to further investigate the disorder effect of a single Zn impurity, we calculate the local density of states (LDOS) spectra near the impurity site. The LDOS can be expressed as

$$\rho_i(\omega) = \sum_{n,\alpha} \left[|u_{i\alpha}^n|^2 \delta(E_n - \omega) + |v_{i\alpha}^n|^2 \delta(E_n + \omega) \right], \quad (8)$$

where the delta function $\delta(y) = \Gamma/\pi(y^2 + \Gamma^2)$, and $\Gamma = 0.004$ is the quasiparticle damping. A 32×32 supercell is taken to calculate the LDOS. Two in-gap resonance peaks [42] emerge below and above the Fermi energy E_f at the impurity site, nearest-neighbor (NN) sites, and the NNN sites, as shown in Figs. 3(c) and 3(d). The LDOS curves at these sites are similar. The intensity of the peak below E_f is higher than that of the right peak above E_f. Moreover, the intensity of the peak below E_f is the highest in the NNN site, then lower in the NN site, and finally in the impurity site.

IV. SDW SUPPRESSION WITH THE EXISTENCE OF ZINC IMPURITIES

We have studied the effect of substituted-Zn ions on the SDW order in doped $\text{Ba}(\text{Fe}_{1-x}\text{Zn}_x)_2\text{As}_2$. First, we focus on the single impurity effect on the underdoped systems. We put our single substituted Zn at the center, $I_m = (14, 14)$. According to the phase diagram [Fig. 1(c)], we choose the system at two different doping levels, $n = 1.90$ and $n = 2.05$, respectively. These two systems show the coexistence of collinear AFM SDW and SC. Figures 4(a) and 4(b) show the spatial profiles of local magnetic order with a single substituted-Zn ion. Numerically, in the system at $n = 1.90$, the AFM SDW is not as stable, but it is obvious. Both cases give similar results:

(a) $n = 1.80$
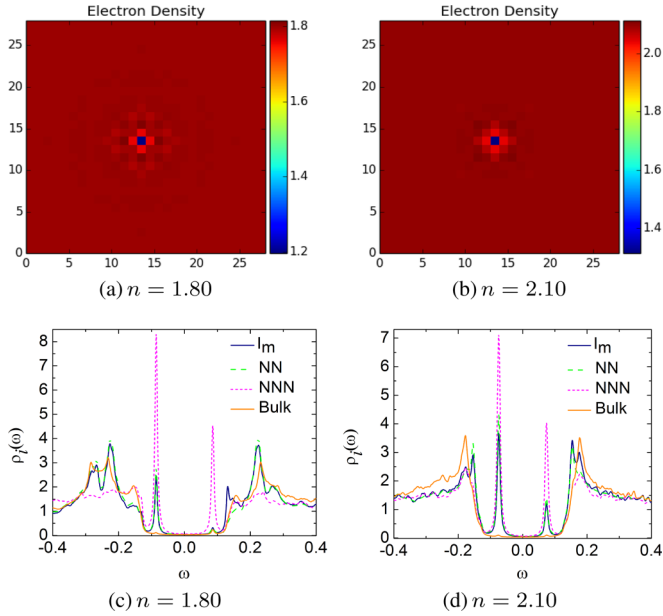
(b) $n = 2.10$

(c) $n = 1.80$

(d) $n = 2.10$

FIG. 3. Spatial profiles of local electron density with a single substituted-Zn ion at the center $I_m = (14, 14)$ at different doping levels: (a) $n = 1.80$, (b) $n = 2.10$. Corresponding LDOS spectra with (c) $n = 1.80$, (d) $n = 2.10$. The blue solid lines represent the LDOS at the impurity site. The green dashed lines show the LDOS at the NN site of the impurity site. The magenta short dashed lines show the LDOS at the NNN site of the impurity site. The orange solid lines show the LDOS at the site far away from the impurity.

(a) $n = 1.90$

(b) $n = 2.05$

(c) $n = 1.90$

(d) $n = 2.05$
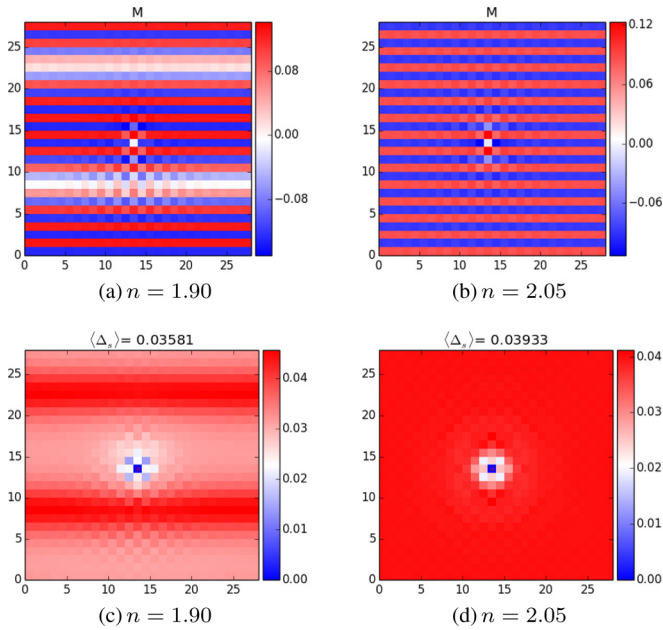
FIG. 4. Spatial profiles of local magnetic order parameter M with a single substituted-Zn ion at $I_m = (14, 14)$, at different doping levels: (a) $n = 1.90$, (b) $n = 2.05$. Spatial profiles of the local superconductivity order parameter Δ_s with a single substituted-Zn ion at $I_m = (14, 14)$, at different doping levels: (c) $n = 1.90$, (d) $n = 2.05$. $\langle \Delta_s \rangle$ represents the averaged value of Δ_s.
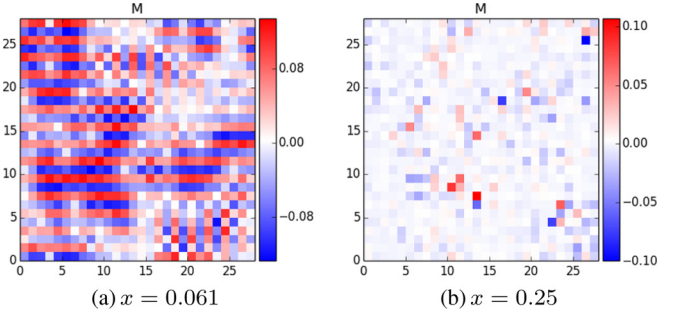
(a) $x = 0.061$

(b) $x = 0.25$

FIG. 5. Spatial profiles of local magnetic order parameter M at a doping level $n = 2.00$, with different concentrations of substituted-Zn ions: (a) $x = 0.061$, (b) $x = 0.25$.

There is no magnetic order at the substituted-Zn atom, while there is a marginally suppressed magnetic order at the adjacent Fe sites.

According to the suppression of AFM SDW in the system with a single impurity, we investigate the multi-impurity cases. Previous discussions show that substituted Zn in the $Ba(Fe_{1-x}Zn_x)_2As_2$ system provides electrons into the system. Thus the effect on the AFM SDW of multi-substituted-Zn system comes from the scattering of substituted Zn, when, meanwhile, the effect also comes from the change in doping level in the system. The SDW in the hole-doped region is complicated. It will be suppressed until the concentration of substituted-Zn ions is a relatively large value in the system. Correspondingly, we choose $n = 2.00$ to study the SDW order. Figure 5 shows the spatial profiles of the local magnetic order parameter with different Zn-concentration ratios x. With $x = 0.061$, the strength of the local magnetic order parameter is suppressed in the occupied substituted-Zn ion areas, while in the few-substituted-Zn ion areas, the collinear AFM SDW is still distinct. Although in our discussions the interactions between Zn impurities are neglected while we avoid excessive concentrations of impurities in an area, we still calculate the case with $x = 0.25$. As shown in Fig. 5(b), the SDW is completely destroyed, which is consistent with the experimental results [20].

V. SUPERCONDUCTIVITY SUPPRESSION WITH THE INCREASE OF ZINC IMPURITIES

In the following, we study the effect of substituted-Zn ions on the SC order parameter at different doping levels. First, we focus on a single substituted-Zn ion at the center of the lattice site $I_m = (14, 14)$ at two different doping levels: $n = 1.90$ and $n = 2.05$. Figures 4(c) and 4(d) illustrate the spatial profiles of the local SC order parameter in each case, respectively. It is very clear that the SC order parameter on the adjacent sites is suppressed around the substituted-Zn ion.

We investigate the effect of multi-Zn impurities on SC with different x at the electron- and hole-doped regions, respectively. According to Fig. 6, the SC is suppressed because of the substituted-Zn ions in the $Ba(Fe_{1-x}Zn_x)_2As_2$ system, regardless of the doping level. In the electron-doped region [Figs. 6(a)–6(d)], with $x = 0.01$, our results show the SC order is suppressed around the substituted-Zn ions, while with $x = 0.061$, the SC order becomes localized, and the

(a) $n = 2.05$, $x = 0.01$

(b) $n = 2.10$, $x = 0.01$

(c) $n = 2.05$, $x = 0.061$

(d) $n = 2.10$, $x = 0.061$

(e) $n = 1.80$, $x = 0.01$

(f) $n = 1.90$, $x = 0.01$

(g) $n = 1.80$, $x = 0.03$

(h) $n = 1.90$, $x = 0.03$
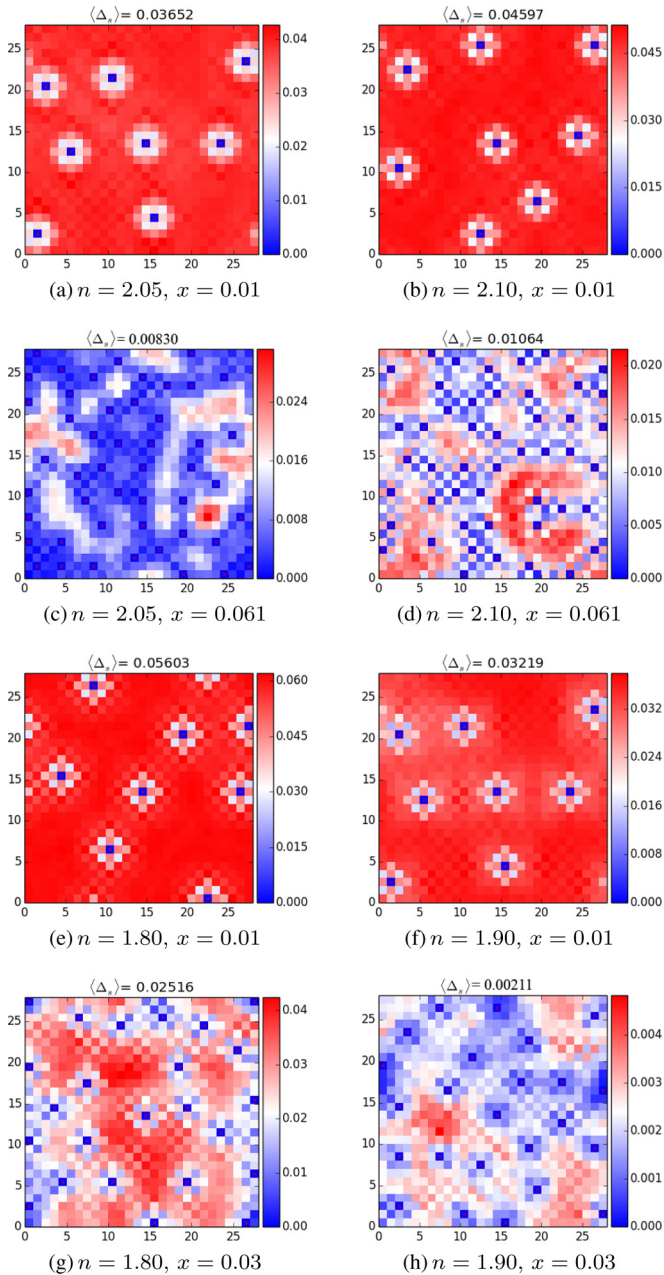
FIG. 6. Spatial profiles of local SC order parameter Δ_s with different conditions. $\times$ (red) represents the position of the substituted-Zn ions. $\langle \Delta_s \rangle$ represents the averaged value of Δ_s.

high intensity spots of the SC order parameter appear most likely in the Zn-free areas. Similar results are obtained in the hole-doped region [Figs. 6(e)–6(h)]. However, the SC is severely suppressed in the hole-doped region. At $n = 1.90$ and with $x = 0.03$, the SC order is nearly destroyed.

Furthermore, we averaged over 20 different impurity configurations for each doping level n and Zn-concentration ratio x. Then we obtain the dependence of the averaged SC order parameters on different x in the Ba(Fe$_{1-x}$Zn$_x$)$_2$As$_2$ system at a certain doping level n, as shown in Fig. 7. Figure 7(a) illustrates the relation in the electron-doped region. SC order linearly decreases with increasing substituted-Zn ions in the Ba(Fe$_{1-x}$Zn$_x$)$_2$As$_2$ system. Around $x = 0.08$, the SC roughly

(a) electron-doped region
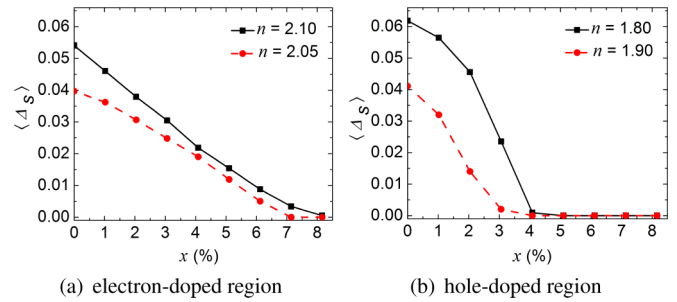
(b) hole-doped region

FIG. 7. Averaged SC order vs the ratio of substituted-Zn ions in the Ba(Fe$_{1-x}$Zn$_x$)$_2$As$_2$ system in the (a) electron-doped region and (b) hole-doped region.

disappears, regardless of whether the doping level is in the optimally doped ($n = 2.10$) or the underdoped ($n = 2.05$) region. These results agree well with the experiments [15,16]. Figure 7(b) shows the relation in the hole-doped region. The trend for decreasing SC order is different from that in the electron-doped region. The SC is more severely suppressed, and then destroyed with a smaller Zn-concentration ratio x in the system. Our calculations give comparable results with recent experiments [14], which show that SC in the hole-overdoped BaFe$_2$As$_2$ almost disappears around $x = 0.03$.

VI. CONCLUSION AND DISCUSSIONS

In a previous study [12] of the effect of the Zn impurities on the superconductivity (SC) in BaFe$_2$As$_2$, the authors considered the optimally electron-doped ($n \sim 2.13$) BaFe$_2$As$_2$ without SDW order, and assumed the substituted Zn behaves as an isovalent impurity and does not provide charge carriers into the system. By adjusting the hopping integrals between nearest-neighboring Fe ions around the substituted-Zn impurity, Ref. [12] is able to account for the suppression of SC as a function of Zn concentration, as observed in experiment [16]. However, using the same method and the local band parameters [12] to examine the effect of Zn impurities on the SC for the underdoped ($n = 2.05$) system with coexisting SDW order, we found that the obtained SC order appears to drop much faster as a function of Zn concentration, when compared with the experimental measurements [16]. This motivates us to reexamine the nature of Zn in doped BaFe$_2$As$_2$. Although experiments showing how large the valence of the Zn impurity should be are lacking, a recent DFT work [43] indicates that Zn provides an effective number of additional electrons into the system. We believe the additional electron should not come from the Zn 3d orbitals. Thus we perform first-principles calculations and resolve the projected partial Fe 3d, Fe 4s, Zn 3d, and Zn 4s density of states in the substituted-Zn BaFe$_2$As$_2$ system. Our results indicate that the Zn 3d orbitals are far below the Fermi energy, while the Zn 4s level is narrowly distributed above and below the Fermi energy, and, more importantly, the empty Zn 4s energy is not far above the Fermi energy. Thus the substituted Zn should not be isovalent, which is different from conventional understanding. For the sake of convenience, we choose the proper local band parameters to make the valence

of Zn close to 1. With this assumption, we are able to account for the suppressions of SC by Zn impurities in both electron- and hole-doped $BaFe_2As_2$ with and without SDW order as measured by experiments [14–16] using the same set of local band parameters.

[1] A. S. Sefat, R. Y. Jin, M. A. McGuire, B. C. Sales, D. J. Singh, and D. Mandrus, Phys. Rev. Lett. **101**, 117004 (2008).

[2] L. J. Li, Y. K. Luo, Q. B. Wang, H. Chen, Z. Ren, Q. Tao, Y. K. Li, X. Lin, M. He, Z. W. Zhu, G. H. Cao, and Z. A. Xu, New J. Phys. **11**, 025008 (2009).

[3] M. Rotter, M. Tegel, and D. Johrendt, Phys. Rev. Lett. **101**, 107006 (2008).

[4] S. Avci, O. Chmaissem, J. M. Allred, S. Rosenkranz, I. Eremin, A. V. Chubukov, D. E. Bugaris, D. Y. Chung, M. G. Kanatzidis, J.-P. Castellan, J. A. Schlueter, H. Claus, D. D. Khalyavin, P. Manuel, A. Daoud-Aladine, and R. Osborn, Nat. Commun. **5**, 3845 (2014).

[5] P. W. Anderson, J. Phys. Chem. Solids **11**, 26 (1959).

[6] A. A. Abrikosov and L. P. Gor'kov, Zh. Eksp. Teor. Fiz. **39**, 1781 (1960) [Sov. Phys. JETP **12**, 1243 (1961)].

[7] J. M. Tarascon, L. H. Greene, P. Barboux, W. R. McKinnon, G. W. Hull, T. P. Orlando, K. A. Delin, S. Foner, and E. J. McNiff, Jr., Phys. Rev. B **36**, 8393 (1987).

[8] Y. Bang, H. Y. Choi, and H. Won, Phys. Rev. B **79**, 054529 (2009).

[9] S. Onari and H. Kontani, Phys. Rev. Lett. **103**, 177001 (2009).

[10] Z.-J. Yao, W.-Q. Chen, Y.-K. Li, G.-H. Cao, H.-M. Jiang, Q.-E. Wang, Z.-A. Xu, and F.-C. Zhang, Phys. Rev. B **86**, 184515 (2012).

[11] Y. K. Li, C. Y. Shen, Y. K. Luo, X. J. Yang, Q. Tao, G.-H. Cao, and Z.-A. Xu, Europhys. Lett. **102**, 37003 (2013).

[12] H. Chen, Y.-Y. Tai, C. S. Ting, M. J. Graf, J. Dai, and J.-X. Zhu, Phys. Rev. B **88**, 184509 (2013).

[13] L. Pan, J. Li, Y.-Y. Tai, M. J. Graf, J.-X. Zhu, and C. S. Ting, Phys. Rev. B **90**, 134501 (2014).

[14] J. Li, M. Ji, T. Schwarz, X. X. Ke, G. V. Tendeloo, J. Yuan, P. J. Pereira, Y. Huang, G. F. Zhang, H.-L. Feng, Y.-H. Yuan, T. Hatano, R. Kleiner, D. Koelle, L. F. Chibotaru, K. Yamaura, H.-B. Wang, P.-H. Wu, E. Takayama-Muromachi, J. Vanacken, and V. V. Moshchalkov, Nat. Commun. **6**, 7614 (2015).

[15] J. Li, Y. Guo, S. Zhang, S. Yu, Y. Tsujimoto, H. Kontani, K. Yamaura, and E. Takayama-Muromachi, Phys. Rev. B **84**, 020513(R) (2011).

[16] J. Li, Y. Guo, S. Zhang, Y. Tsujimoto, X. Wang, C. I. Sathish, S. Yu, K. Yamaura, and E. Takayama-Muromachi, Solid State Commun. **152**, 671 (2012).

[17] L. J. Zhang and D. J. Singh, Phys. Rev. B **80**, 214530 (2009).

[18] H. Wadati, I. Elfimov, and G. A. Sawatzky, Phys. Rev. Lett. **105**, 157004 (2010).

[19] T. Berlijn, C.-H. Lin, W. Garber, and W. Ku, Phys. Rev. Lett. **108**, 207003 (2012).

[20] S. Ideta, T. Yoshida, M. Nakajima, W. Malaeb, T. Shimojima, K. Ishizaka, A. Fujimori, H. Kimigashira, K. Ono, K. Kihou, Y. Tomioka, C. H. Lee, A. Iyo, H. Eisaki, T. Ito, and S. Uchida, Phys. Rev. B **87**, 201110(R) (2013).

[21] The first-principles calculations presented in this work were performed using the all-electron full potential linear augmented plane wave plus local orbitals method [22] as implemented in the WIEN2K code [23]. The exchange-correlation potential was calculated using the generalized gradient approximation as proposed by Pedrew, Burke, and Ernzerhof [24]. These calculations were perform using the optimized 2×2 supercell structure with one Fe atom substituted by Zn.

[22] D. J. Singh and L. Nordstrom, *Planewaves, Pseudopotentials, and the LAPW Method*, 2nd ed. (Springer, Berlin, 2006), pp. 1–134.

[23] P. Blaha, K. Schwarz, G. Madsen, D. Kvasnicka, and J. Luitz, in *WIEN2K, An Augmented Plane Wave + Local Orbitals Program for Calculating Crystal Properties*, edited by K. Schwarz (Technical University Wien, Austria, 2001).

[24] J. P. Perdew, K. Burke, and M. Ernzerhof, Phys. Rev. Lett. **77**, 3865 (1996).

[25] D. G. Zhang, Phys. Rev. Lett. **103**, 186402 (2009).

[26] Y.-Y. Tai, J. X. Zhu, M. J. Graf, and C. S. Ting, Europhys. Lett. **103**, 67001 (2013).

[27] S. Raghu, X.-L. Qi, C.-X. Liu, D. J. Scalapino, and S.-C. Zhang, Phys. Rev. B **77**, 220503(R) (2008).

[28] K. Kuroki, H. Usui, S. Onari, R. Arita, and H. Aoki, Phys. Rev. B **79**, 224511 (2009).

[29] M. S. Laad and L. Craco, Phys. Rev. Lett. **103**, 017002 (2009).

[30] F. Wang, H. Zhai, and D.-H. Lee, Phys. Rev. B **81**, 184512 (2010).

[31] R. Thomale, C. Platt, W. Hanke, and B. A. Bernevig, Phys. Rev. Lett. **106**, 187003 (2011).

[32] Y. H. Su, C. Setty, Z. Q. Wang, and J. P. Hu, Phys. Rev. B **85**, 184517 (2012).

[33] J. P. Hu and N. Hao, Phys. Rev. X **2**, 021009 (2012).

[34] H. Ding, P. Richard, K. Nakayama, K. Sugawara, T. Arakane, Y. Sekiba, A. Takayama, S. Souma, T. Sato, T. Takahashi, Z. Wang, X. Dai, Z. Fang, G. F. Chen, J. L. Luo, and N. L. Wang, Europhys. Lett. **83**, 47001 (2008).

[35] I. I. Mazin, D. J. Singh, M. D. Johannes, and M. H. Du, Phys. Rev. Lett. **101**, 057003 (2008).

[36] F. Wang, H. Zhai, Y. Ran, A. Vishwanath, and D.-H. Lee, Phys. Rev. Lett. **102**, 047005 (2009).

[37] H. Huang, D. G. Zhang, T. Zhou, and C. S. Ting, Phys. Rev. B **83**, 134517 (2011).

[38] Y. Y. Zhao, Y.-Y. Tai, and C. S. Ting, Phys. Rev. B **91**, 205110 (2015).

[39] A. M. Oles, G. Khaliullin, P. Horsch, and L. F. Feiner, Phys. Rev. B **72**, 214431 (2005).

[40] D. K. Pratt, W. Tian, A. Kreyssig, J. L. Zarestky, S. Nandi, N. Ni, S. L. Bud'ko, P. C. Canfield, A. I. Goldman, and R. J. McQueeney, Phys. Rev. Lett. **103**, 087001 (2009).

[41] S. Avci, O. Chmaissem, D. Y. Chung, S. Rosenkranz, E. A. Goremychkin, J. P. Castellan, I. S. Todorov, J. A. Schlueter, H. Claus, A. Daoud-Aladine, D. D. Khalyavin, M. G. Kanatzidis, and R. Osborn, Phys. Rev. B **85**, 184507 (2012).

[42] T. Zhou, H. X. Huang, Y. Gao, J.-X. Zhu, and C. S. Ting, Phys. Rev. B **83**, 214502 (2011).

[43] S. N. Khan, A. Alam, and D. D. Johnson, Phys. Rev. B **89**, 205121 (2014).